SURFACE MODIFICATION OF MAGNETIC NANOPARTICLES FOR FORMULATION OF PHOTOLUMINESCENT POLYMER-COATED MAGNETIC NANOPARTICLES TO DETECT AND TREAT CANCERS

by

TEJASWI D. KADAPURE

Presented to the Faculty of the Graduate School of

The University of Texas at Arlington in Partial Fulfillment

of the Requirements

for the Degree of

MASTER OF SCIENCE IN BIOMEDICAL ENGINEERING

THE UNIVERSITY OF TEXAS AT ARLINGTON

August 2012

ACKNOWLEDGEMENTS

John Crosby said, “Mentoring is a brain to pick, an ear to listen and a push in the right direction,” thus rightly defining Dr. Kytai Truong Nguyen as a mentor. I am thankful to Dr. Nguyen for offering me an opportunity to work in her laboratory. Dr. Nguyen was a constant source of inspiration and guidance that enabled me to achieve my research goals. Her words “treat your research as your baby” have refined me as a researcher and will always remain an inspirational quote throughout my career.

I am very thankful to Dr. Jian Yang for collaborating with us on this project, guiding me throughout this work and serving on my thesis committee. I would also like to thank Dr. Baohong Yuan for serving on my thesis committee and reviewing my research work. Most importantly, I would like to extend my gratitude to Aniket Wadajkar, the man who was the strong pillar throughout my master program. He was an inspiration to achieve great heights, to do something that I thought I couldn’t, to believe in myself and to face all the rough patches with a smile. If I was to describe Aniket, I would say that he is the best friend, philosopher, and guide I’ve ever had. I would like to specially acknowledge Sonia Santimano, despite sailing in the same boat she was extremely helpful, loving and supportive. Additionally, I would like to thank my best friends Uday Tata, Roshni Iyer and Micheal Palmer for their constant love, support, guidance and help throughout my research. I would also like to thank all the lab members, Dr. Zhiew Xie, Lee-chun Su, Jyothi Menon, Pranjali Tambe, and Parth Jadeja for providing a healthy research environment.

Finally, I would say Thank you Mom and Dad, I would not have been here achieving this success if it would not have been for your unconditional love and support throughout. I am grateful to my brother for being supportive and a best buddy throughout my life. Lastly, I am very happy to express my gratitude to my fiancé, Nikhil Aphale, for his constant love and emotional support.

July 17, 2012

ABSTRACT

SURFACE MODIFICATION OF MAGNETIC NANOPARTICLES FOR FORMULATION OF PHOTOLUMINESCENT POLYMER-COATED MAGNETIC NANOPARTICLES TO DETECT AND TREAT CANCERS

Tejaswi Dhanpal Kadapure, M.S.

The University of Texas at Arlington, 2012

Supervising Professor: Kytai Truong Nguyen

Cancer has been one of the leading causes of death worldwide that necessitates the development of theranostic systems for effective cancer management. Previously, we developed biodegradable-photoluminescent polymer coated magnetic nanoparticles (BPLP-MNPs) as a theranostic system for cancer management. These BPLP-MNPs were highly stable with excellent biocompatibility and consisted of magnetic targeting and imaging capabilities. However, these particles experienced reduced fluorescence due to the presence of dark/blackness of MNPs, which absorbs excited/emitted light. Therefore, it was hypothesized that surface modification on MNPs can overcome this limitation and enhance fluorescence for BPLP-MNPs.

The goal of this research was therefore to employ various surface coatings such as silane (Si), hydroxypatite (HA), or Si with azide on MNPs prior to formulation of BPLP-MNPs and investigate if the surface modification of MNPs would improve their properties, particularly the fluorescent properties. Modified MNPs were used to formulate BPLP-MNPs by either standard emulsion or click chemistry techniques. The obtained BPLP-coated surface modified MNPs (BSM-MNPs) with a diameter range of 200-350 nm were stable and biocompatible. Additionally, Fourier Transform Infra-Red (FTIR) spectra analysis and Transmission Electron Microscopy (TEM) confirmed the chemical and morphological structures of BSM-MNPs. The particles possessed superparamagnetic properties and provided excellent

contrast for magnetic resonance imaging (MRI). In addition, all BSM-MNPs had excellent fluorescence intensity compared to that of BPLP-MNPs. The further analysis of fluorescence intensity *in vitro* and *in vivo* optical imaging of the particles indicated that MNP-HA-BPLP particles exhibited best fluorescence amongst BSM-MNPs. MNP-HA-BPLP particles were further used for therapeutic applications.

To study the potential use of MNP-HA-BPLP nanoparticles as a drug carrier, anti-cancer drugs such as Paclitaxel and Docetaxel were used as drug models. MNP-HA-BPLP particles could deliver 80% of loaded drug over a period of 21 days and were uptaken by cancer cells in a dose-dependent manner, Furthermore, MNP-HA-BPLP-drug loaded particles effectively reduced cancer cell growth, supporting their use for cancer treatment. In conclusion, MNP-HA-BPLP forms an efficient theranostic system with excellent dual imaging and therapeutic capabilities. Future studies include extensive work on *in vivo* therapeutic efficacy of MNP-HA-BPLP particles.

TABLE OF CONTENTS

LIST OF ILLUSTRATIONS

Figure Page

LIST OF TABLES

CHAPTER 1

INTRODUCTION

1.1 Cancer Overview

Cancer is typically defined as the uncontrolled and rapid division of cells resulting from a mutation in genes that are responsible for slowing down the cell cycle. Moreover, inability to pause for DNA repair and loss of control over telomere length altogether leads to the unregulated growth of cells and subsequent deaths [1]. Most cancers, including prostate, skin, and thyroid cancers, can easily metastasize to other organs if not detected and treated at an early stage, leading to significant life shortening [2-4]. In order to treat cancer, many therapies are available that include surgery, hormone therapy, radiation therapy, chemotherapy, and so on. However, these therapies have many disadvantages such as nausea, hair loss, weakness and dysfunctions of the organs, leading to a low quality of life for cancer patients. The mentioned drawbacks from conventional therapies have provoked a need for the development of new strategies to achieve better cancer management with the effective killing of cancer cells, while having minimal side-effects. In order to accomplish this goal, there has been an extensive research in the field of Nanotechnology.

The history of nanotechnology dates back to 1959 when a famous Physicist, Richard Feynman, had explained the concept of nanotechnology at an American Physical Society meeting [47]. He described a method by which individual atoms and molecules could be manipulated with the help of precise tools in this meeting. However, the term Nanotechnology was first defined by Professor Norio Taniguchi (1974) in his paper, which described the processing, separation, consolidation and deformation of materials by one atom or molecule [47]. Thereafter, nanotechnology was explored extensively and has been one of the major research areas in the field of cancer diagnosis and therapy.

1.2 Nanoparticles as Drug Carriers

Nanotechnology has offered a diverse platform with exceptional nanodevices classified as organic and inorganic materials [5]. One of such nanodevices are nanoparticles, which are extensively researched as drug delivery systems for the treatment of cancer. Nanoparticles are minuscule particles with a size less than 1000 nm, which possess excellent physicochemical properties, facilitating its use for successful delivery of therapeutic agents [6]. Nanoparticles also allow site specific and programmed delivery of drugs to overcome limitations of systemic delivery of therapeutic agents, such as causing toxicity to other healthy areas and reducing the bioavailability of the drugs at the site of disease. Due to reduced bioavailability of drugs, multiple administrations of these agents become mandatory to achieve all the necessary functions [7]. Nanoparticles are therefore an efficient drug delivery device which can be tailored to achieve maximum therapeutic effects at the diseased site [8]. Moreover, the small size of nanoparticles ensures convenient and uninterrupted interactions with biological systems at molecular levels [6]. Furthermore, the small size offers a higher surface area to volume ratio than larger particles of the same composition, allowing higher encapsulation of the drug [8]. Lastly, solubility and stability of nanoparticles can be improved by encapsulating or binding other molecules and materials such as aptamers [9], peptides [10], antibodies [11], and natural [12] and synthetic polymers [13, 14].

Although nanoparticles have many advantages, there are certain disadvantages which might limit their use. First of all, particles of a size less than 10 nm are easily cleared from the body through renal passages, whereas particles of a size greater than 500nm are often taken up/eliminated by the macrophages or reticuloendothelial system (RES) [15]. Moreover, if the material used to synthesize nanoparticles is non-degradable, it may accumulate in the body, leading to long term toxicity for the patient [16]. However, these limitations of nanoparticles can be overpowered by the use of biodegradable and biocompatible materials [17]. Additionally, controlled synthesis procedures can produce particles of appropriate sizes, thus increasing the circulation time in the body [8]. Furthermore, targeting nanoparticles directly to the diseased site would also avoid the elimination by RES [15]. Thus, the ability

to conquer the disadvantages associated with nanocarriers has led to the development of various nanoparticulate drug delivery systems.

Several types of nanoparticles, including liposomes, polymeric nanoparticles, and inorganic (metallic/ceramic) nanoparticles have been developed due to many advantages as listed above [17]. Of those nanoparticulate systems, liposomes comprise an aqueous core surrounded by lipid bilayer membrane, and provide an improved drug efficacy and safety, as properties of compounds used for their preparation are similar to biological membranes in nature. Stealth liposomes developed by conjugation of Poly(ethylene glycol) (PEG) easily escape the interception of immune systems, thus achieving longer circulation time [18]. Another class of nanoparticles is polymeric nanoparticles made of either synthetic or natural polymers, or both. They allow encapsulation or conjugation of drugs and targeting ligands, thus facilitating site specific targeting and providing a desired level of therapy [16, 17]. Additionally, imaging agents can be embedded in the polymer shell and permit optical imaging at cellular levels. Besides these materials, metallic nanoparticles such as iron oxide, gold and other metal based nanoparticles have also been explored extensively. Iron oxide nanoparticles possess superparamagnetic properties enabling magnetic targeting and providing excellent dark contrast as MRI agents. Gold and other metal based nanoparticles have also been investigated for exceptional imaging and therapy applications, especially gold [16]. All the above mentioned capabilities of different nanoparticles have led to an extensive research in the field of cancer management with use of nanoparticles called as ‘theranostic’ nanoparticles.

1.3 Theranostic Particles

Theranostic particles as the name suggests offer therapy and diagnosis simultaneously. One of these particles is magnetic-based theranostic particles (MBTP) that contain a special component, iron oxide nanoparticles. Magnetic nanoparticles (MNPs) possess all properties of targeting, imaging and therapy thus proving to be the perfect drug carrier. However, magnetic nanoparticles cannot be used as an effective drug carrier by itself due its unstable nature, leading to aggregation as a result of high surface energy [19]. Also, nanoparticles are about 9-10 nm in size and can be easily cleared through renal

passages. Nevertheless, MNPs can be functionalized or coated with biodegradable and biocompatible polymers to increase its stability and solubility [17, 20]. Additionally, drugs or fluorescent imaging agents can be loaded within the polymer shell that can simultaneously aid in providing a sustained release of drug and optical imaging along with MRI [5, 6, 20, 21]. Figure 1.1 below describes several aspects of magnetic based theranostic particles that prove them ideal for cancer management.

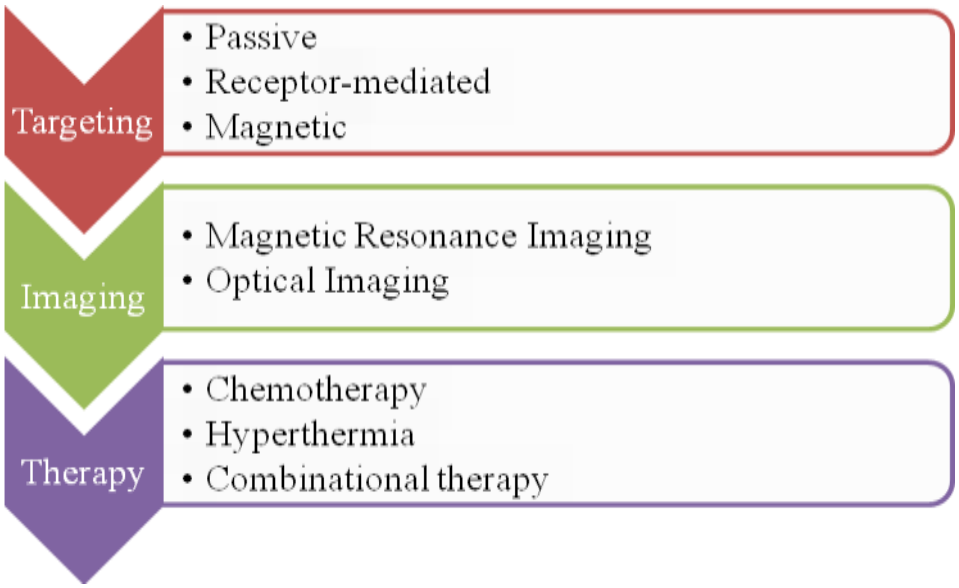

Figure 1.1 Schematic diagram representing all the aspects of Magnetic-based Theranostic particles (MBTP)

1.3.1 Targeting

Targeting is the most important aspect of any drug delivery system as it helps in avoiding systemic toxicity and rapid clearance from the body [22]. Three major routes of targeting are passive, active, and magnetic targeting. Passive targeting basically relies on the enhanced permeation and retention (EPR) effect through the tumor leaky vasculature and undeveloped defective lymphatic system [23]. EPR effect allows the easy penetration and accumulation of nanoparticles in the tumor as particles fail to return to systemic circulation due to damaged lymphatic drainage system [24]. However, passive targeting may be ineffective as particles may get cleared through renal passages and RES quickly.

In order to achieve efficient targeting, active targeting of nanoparticles to cancerous cells is possible with the help of either targeting ligands or magnetic nanoparticles. Targeting ligands, which are binding to the surface markers expressed by cancer cells only, can be conjugated on the particle surface thus ensuring the delivery of nanoparticles to the tumor for specific drug delivery. Nanoparticles, once attached onto the cell surface, are uptaken by cells through receptor-mediated endocytosis, inducing programmed cell death to cancer cells only through the drug released from the nanoparticles [23]. Thus with the use of specific targeting strategies, bioavailability of the drug can be increased drastically [15]. Conversely, magnetic targeting can be specifically used for localized nanoparticles at the specific area as the external magnetic field is applied particularly at the tumor site to facilitate nanoparticle accumulation in the tumor, due to the superparamagnetic behavior of MNPs [25].

1.3.2 Imaging

Imaging throughout the course of treatment is an important means by which a clear analysis of particle biodistribution and pharmacokinetic activity of drugs used can be obtained [26]. Besides, the amount of drug to be administered can be tailored based on the observation of treatment responses. Typically, the use of two imaging modalities simultaneously would provide an enhanced and precise analysis of tumor size and location [27]. Magnetic resonance imaging and optical imaging are two modalities that have been commonly used together, as MRI acquired using magnetic nanoparticles provides extraordinary dark contrast and penetration depth, thus highlighting the tumor outline precisely [28]. Optical imaging, on the other hand, provides high sensitivity and is useful for molecular imaging [29].

Several optical imaging agents such as Quantum Dots (QDs) and fluorescent dyes have been developed and used for encapsulation within MBTPs to achieve dual imaging modalities. QDs have been one of the most popular contrast agents for optical imaging as they provide broader excitation spectra with a sharp defined emission peak, offering excellent fluorescence even at deeper tissues [30]. Similarly, fluorophores and fluorescent dyes such as fluorescein and DiL/DiR have been encapsulated or conjugated

with MNPs for both MRI and optical imaging applications [31]. Despite all of these functions, optical imaging reagents are either toxic in nature and can't be used for humans, or undergo photobleaching, which reduces the fluorescent signal over the time [32]. These limitations entice a need for the development of imaging agents that are biocompatible and can provide stable fluorescence signals for longer periods. Previous work in our group has developed a family of amino-acids based on biodegradable photoluminescent polymers (BPLPs), which exhibit fluorescence inherently, thus avoiding the conjugation of any fluorescent organic dyes or QDs [33]. BPLPs have various advantage properties like biodegradability, biocompatibility, and superior photoluminescence [33], suggesting that these materials can be used for formulation of an excellent MBTP.

1.3.3 Therapy

Chemotherapy and hyperthermia, with the aid of MBTP, are two therapeutic strategies that can facilitate the destruction of cancer cells with minimal damage to healthy areas. Anti-cancer drugs such as doxorubicin, docetaxel, gemcitabine, cisplatin, and so on can be encapsulated within the polymer shell of MBTP so that a controlled and sustained release of drug at the cancer site can be achieved. Other than anti-cancer drugs, bioactive molecules can also be delivered with the help of MBTPs to reduce tumor growth. Additionally, hyperthermia can also be used as a therapeutic tool that involves use of an excess heat produced by MNPs, owing to their metallic and magnetic properties to kill cancer cells [34]. Upon application of an alternating magnetic field, MNPs tend to vibrate, producing thermal energy, and this thermal energy increases the temperature above 41˚C [35]. The heat generated by MNPs can lead the cancer cells to undergo apoptosis and be controlled by modulating certain factors such as magnetic properties, particles sizes, amplitude and frequency of applied magnetic fields [36].

Combinational therapy basically consists of combining two therapies to attain a synergistic effect for increasing treatment efficacy. Two therapies that can be combined to achieve maximum therapeutic effect are either chemotherapy and hyperthermia or radiation therapy and hyperthermia. Hyperthermia generates thermal energy, weakening cancer cells and facilitating their response to either

chemotherapeutic payloads or radiation. Thus, effective and improved treatment can be achieved by targeting, imaging and therapeutic properties of the MBTPs.

1.4 Background and Hypothesis

In order to achieve optical imaging along with MRI without the use of current fluorescent probes, BPLP was coated on MNPs to synthesize BPLP-MNPs. These nanoparticles were highly stable and biocompatible with excellent magnetic properties and could serve as an MRI contrast reagent [37]. However, these particles experienced reduced fluorescence due to the presence of MNPs. The blackness of MNPs was speculated to absorb the emitted/excited light, further reducing the fluorescence intensity of BPLP-MNPs. Therefore, it was important to cover the blackness of MNPs prior to formulation of BPLP-MNPs in order to improve fluorescence signals for BPLP-MNPs. Due to this speculation, it was hypothesized that surface modification of MNPs which could cover the blackness of MNPs would enhance the fluorescence of these theranostic nanoparticles. Various surface coatings employed to achieve this goal were Silane (Si) coating, Hydroxypatite (HA) coating, and Si with Azide coating. Figure 1.2 below is the schematic representation of all BSM-MNPs. It can be seen that silane (grey coating) MNPs form the core of MNP-Si-BPLP-BPLP, while, HA (white coating) on MNPs form the core of MNP-HA-BPLP respectively, with polymer forming the shell. Further, Silane-Azide MNPs with BPLP coating employ ‘click chemistry’ to obtain MNP-Click-BPLP particles.

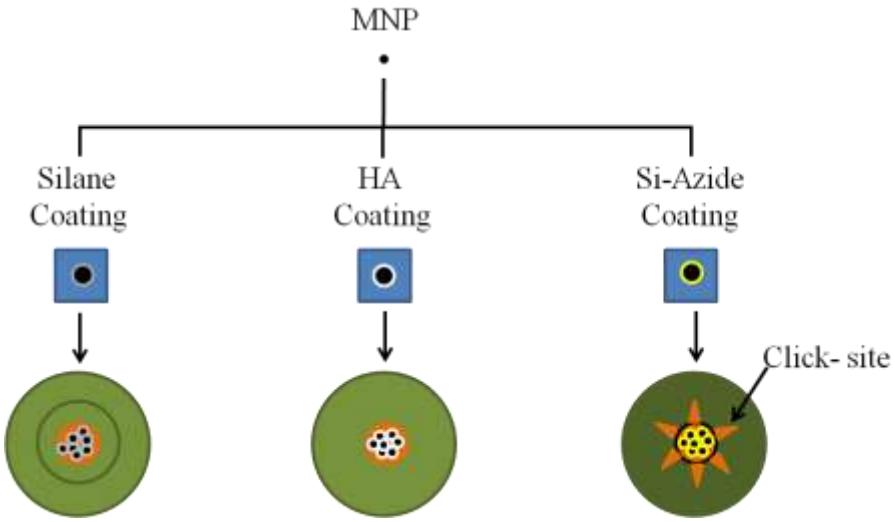

Figure 1.2 Schematic representation of surface modifications employed to synthesize SMB-MNPs

1.5 Objective of this Research

1.5.1 Specific Aims

As explained earlier, BPLP-MNPs would serve as theranostic particles with excellent targeting, dual imaging and effective therapeutic capabilities. However, the optical imaging capability of BPLP-MNPs experiences reduced fluorescence intensity due to blackness of MNPs. Thus, surface modification of MNPs before coating with the BPLP polymer is needed for excellent imaging and therapeutic applications. The two aims sought to accomplish this goal were:

- Synthesis and characterization of BPLP-coated surface-modified MNPs (BSM-MNPs).
- Application of the best BSM-MNPs on cancer cell lines to evaluate its therapeutic effects.

1.5.2 Successful Outcomes

The successful outcome of this research would provide profound information as to which surface modified BPLP-coated MNPs would have enhanced optical imaging properties with excellent physicochemical, biological, and magnetic properties. Additionally, results from this research will enhance our knowledge on surface modification of nanoparticles and the relationship of surface

modification with properties of nanoparticles. Finally, if successful, this research will provide more effective theranostic nanoparticles for cancer management.

CHAPTER 2

MATERIALS AND METHODS

2.1 Materials

Materials used for experiments include Magnetic Nanoparticles (MNPs) (Meliorum), Vinyltrimethoxysilane (VTMS) (Sigma Aldrich), Acetic Acid (Sigma Aldrich), Ethanol (99%), Calcium Nitrate Anhydrous (Sigma Aldrich), Potassium Phosphate Monobasic (Sigma Aldrich), CPTES (Sigma Aldrich), DMF (Sigma Aldrich), Copper Sulfate Pentahydrate (Sigma Aldrich), Sodium Azide (Sigma Aldrich), DMSO (Sigma Aldrich), 1,4-Dioxane (Sigma Aldrich), Poly-Lactide Glycolic Acid (PLGA, Lakeshare), Agarose (Sigma Aldrich), Hydrochloric acid (EMD), Potassium Thiocynate (Sigma Aldrich), Ammonium Persulfate (Sigma Aldrich), MTS assay kit (Promega), Paclitaxel (Sigma Aldrich), Docetaxel (Sigma Aldrich) and Pico green DNA assay kit (Promega). Additionally, Adult Human Dermal Fibroblasts (HDFa) was obtained from Invitrogen, and the other cell lines such as HPV7 Prostate Epithelial cells, Skin cancer cells, and thyroid cancer cells were obtained from ATCC. Moreover, culture media used were DMEM (Sigma), RPMI (Gibco; Invitrogen), PrEBM (Lonza), and F12K (ATCC).

2.2 Synthesis of BPLP-coated Surface Modified MNPs (BSM-MNPs)

2.2.1 Synthesis of Biodegradable Photoluminescent Polymer

BPLP was synthesized using citric acid and 1,8 octanediol with L-cysteine as described by Yang et al [33]. Briefly, equal molar amounts of citric acid and 1, 8 octanediol with L-cystein in a molar ratio with citric acid (0.2) were stirred to dissolve at 160˚C for 20 minutes on a magnetic stir plate. After dissolution, temperature was lowered to 140˚C and the solution was continually stirred for 75 minutes. Oligomer thus obtained was further purified by precipitating with 1, 4 Dioxane solution and was lyophilized to obtain BPLP. All BPLPs are synthesized following the same procedure, the only difference

being the monomer used for synthesis of BPLP-alkyne used for making MNP-Click BPLP particles. BPLP-alkyne makes use of propargyl 2, 2 bis (hydroxymethyl) propionate (PHMP).

2.2.2 Silane (Si) coating (MNP-Si)

Si-modified MNPs were obtained by conjugation of vinyltrimethoxysilane onto the surface of MNPs as previously described [38, 39]. Briefly, 0.07424 g of MNPs was dispersed in a mixture of ethanol (99 ml) and DI water (1 ml) by sonicating it for 20 minutes at 40 W. After 10 minutes of sonication, acetic acid (CH_3COOH) was added, and the sonication was continued for another 10 minutes. Once sonication was done, the solution was transferred on to a magnetic stir plate followed by the addition of 0.49 ml vinyltrimethoxysilane, and kept for vigorous stirring for the duration of 24 hours. After reaction, the particles were collected and washed with ethanol solution.

2.2.3 Hydroxypatite (HA) coating (MNP-HA)

HA was coated on magnetic nanoparticles by a precipitation reaction between calcium carbonate and potassium phosphate [40]. Briefly, 164 mg of calcium carbonate ($Ca(NO_3)_2$) was dissolved in 10 ml DI water followed by the addition of 15 mg of iron oxide particles to it. This solution was then sonicated to disperse the magnetic nanoparticles. Further, 81 mg of potassium phosphate was dissolved in 10 ml of DI water and then MNP solution was added to it drop wise. Finally, this solution was treated hydrothermally at a temperature of 200˚C for 20 hours, and obtained HA coated MNPs were washed twice with DI water.

2.2.4 Azide coating (MNP-N_3)

Azide coated MNPs were synthesized using a protocol described by Schlossbauer et al. and Kim et al. [41, 42]. In brief, 50 mg of MNPs in 10 ml Dimethylformamide (DMF) were sonicated for 15 minutes at 20 W and 90% pulse. Subsequently, 50µl of 3-chloropropyltrimethoxysilane (CPTES) was added to the MNP solution, and this solution was sonicated for an hour. The MNPs were then washed

with DMF and resuspended in 20 ml of DMF. Further, 50 mg of sodium azide was added to the MNP solution and stirred for 12 hours at 40˚C. After 12 hours, particles were collected and washed with a series of solvents that include DMF, followed by ethanol and DI water.

2.2.5. Synthesis of MNP-Si-BPLP-BPLP particles

For the synthesis of MNP-Si-BPLP-BPLP particles, double emulsion (water-oil-water) technique was employed twice. In short, 125 mg of BPLP was dissolved in 1.5 ml of 1, 4 dioxane (oil phase) and 10 mg of MNP-Si were dispersed well in 1 ml of DI water (water phase). Simultaneously, 400 mg of SDS was dissolved in 25 ml of DI water (2nd water phase). SDS acts as a surfactant stabilizing the particles and helps restricting the particles to nanometer size. Firstly, polymer solution (oil phase) was added into the oil phase and allowed to sonicate (10 minutes, 40 W), and while sonicating dispersed MNP-Si solution was added drop wise to it. Further, the water-oil emulsified solution of MNP-Si-BPLP was further added to the SDS solution drop wise to form stable nanoparticles. Nanoparticles obtained were washed twice with DI water and the same process was employed on these particles to achieve a second coating of BPLP using double emulsion.

2.2.6 Synthesis of MNP-HA-BPLP particles

MNP-HA-BPLP particles were also synthesized following similar protocol as described above. Briefly, 125 mg of BPLP was dissolved in 1.5 ml of 1, 4 dioxane, 10 mg of MNP-HA were dispersed in 1 ml of DI water and 400 mg of SDS was dissolved in 25 ml of DI water. Firstly, polymer solution was allowed to sonicate and MNP-HA particles dispersed in DI water were added drop wise while sonication was on. Further, the particle–polymer solution was added into the aqueous SDS solution while sonicating. Particles were then collected and washed with DI water.

2.2.7 Synthesis of MNP-Click-BPLP particles

For synthesis of MNP-Click-BPLP particles, 200 mg of BPLP-alkyne was dissolved in 20 ml of Dimethyl sulfoxide (DMSO). Further, 15mg of MNP-N_3 and 50 µl Cu_2O microsphere methanol solution (1.25%) were added, and complete solution was sonicated for 15 minutes. Followed by sonication, the particle suspension was placed on a shaker at 37˚C for 12 hrs to complete the reaction. The particles were further collected and washed with DMSO, 1,4 dioxane, ethanol and DI water in a series. The particles were then lyophilized to obtain the powder form.

2.3 Characterization of BSM-MNPs

Synthesized particles were characterized for physicochemical properties like size, polydispersity and zeta potential using dynamic light scattering (DLS) equipment (Zeta Pals, Brook Heaven Instrument.). Transmission electron microscopy (TEM) was also used to assess the size and structural information of nanoparticles. For this purpose, 0.1 % w/v particle solution was prepared and added on a Foamvar coated copper grid (Biosciences). The grid with nanoparticles embedded on it was placed in TEM (1200 EX Electron Microscope, JEOL) and imaged to observe the particle size and morphology.

Fourier Transform Infra-Red (FTIR) is used for the analysis of all the chemical structures present within nanoparticles. For this purpose, particles were examined for chemical bonds using an FTIR spectroscope (Nicolet -6700, Thermo Fisher Scientific). The results obtained indicated characteristic peaks for various chemical structures that together form the nanoparticles with different surface modifications and polymers.

The stability of particles was further evaluated by suspending the particles in media containing serum and measuring their size and polydispersity over a period of 7 days. Stability study confirms the activity of particles in physiological conditions by providing information related to aggregation and dispersity.

2.4 Magnetic Property Measurement

Measurements of magnetic properties of synthesized nanoparticles include the use of iron assay to determine the iron content and Vibrating Sample Magnetometer (VSM) to assess the magnetic hysteresis loops when the magnetic field was applied. Presence of MNPs aids in magnetic targeting, therefore determination of iron content is necessary. For iron assays, 0.1 % w/v of all BPLP-coated surface-modified MNPs and bare MNPs (to obtain a standard curve) were first dispersed in Di water. 100 µl of each of the samples (n=4) and standards were incubated with 50 % hydrochloric acid at 50˚C for 2 hours. Secondly, upon dissolution of iron, 50 µg of APS was added to each well and placed on a shaker for 15 minutes. After 15 minutes, 100 µl of 0.1 M Potassium Thiocynate was added to each well and placed on shaker for another 15 minutes. Lastly, an absorbance reading was obtained using a UV-vis spectrophotometer (Tecan Ltd,NC) at a wavelength of 520 nm. The absorbance values obtained were plotted to acquire a percentage of iron mass present in all the surface modified particles.

Furthermore, VSM and magnetic targeting were also performed to determine magnetic property. In order to perform VSM, nanoparticles were embedded in wax moulds and mounted on a transparent, non-magnetic rod. The magnetic field was then applied and magnetic hysteresis loops for all BSM-MNPs with bare MNPs as control were obtained. To illustrate the magnetic targeting ability, nanoparticles were dispersed well in DI water, and then an external magnetic field was applied to assess whether the recruitment of the surface modified BPLP coated MNPs under the influence of an external magnetic field occurred.

2.5 Dual Imaging Capabilities

Magnetic nanoparticles have been used as an MRI contrast agent as they provide dark contrast that helps differentiate between a tumor and healthy tissues. However, in this research, MNPs are surface-modified and are encapsulated within a polymer shell, hence it is important to determine the contrast provided by BSM-MNPs. In order to assess their MRI capability, BSM-MNPs were dispersed in agarose gels, and then these gels were placed in a 35 mm volume radio frequency coil of a Varian unity INOVA

4.7T 40cm horizontal MR machine to obtain images of these agarose phantoms. Spin echo pulse sequence was used for acquiring multi-slice T2 weighted images with specification TR=2000 msec; TE=15msec; field view of 30mm×30mm; matrix= 128×128; slice thickness=2mm.

Furthermore, to verify the effect of BSM-MNPs on fluorescence intensity, particles were imaged under an enhanced optical microscope. Fluorescence emitted by the particles was viewed under an enhanced optical fluorescent microscope (Nikon). For this experiment, 0.2% w/v particles were suspended in an aqueous medium and a drop of this solution was added on a glass slide; and the water was allowed to evaporate to obtain dry particles on the glass slide. Subsequently, particles were covered with a cover slip using a mounting media and were observed under the microscope to obtain fluorescent images. Additionally, photoluminescence spectra of these particles were also obtained using a SHIMADZU RF-5301PC fluoro-spectrophotometer. The optimal emission wavelength was first determined from excitation spectra and then all emission spectra were obtained on the basis of optimal excitation wavelength. Both the excitation and emission slit width were set at 5nm×5nm for all samples unless otherwise stated.

2.6 Cell culture and Biocompatibility Study

2.6.1 Cell Culture Techniques

Various cell cultures such as Adult Human Dermal Fibroblasts (HDFa), Prostate Epithelial cells (HPV7), Thyroid cancer cell lines (KAT-4 & TT cells), Prostate cancer cell lines (PC3 & LNCaP), and Skin cancer cell line (G361), were used in this research. Different cell lines have different growth requirements and thus need different growth mediums; however, incubation conditions such as 37˚C temperature and 5 % CO_2 concentration remain constant. HDFa, KAT-4, and G361 were grown in DMEM media, HPV7 were grown in Pr EBM, TT cells were grown in F12K, and both prostate cancer cell lines were grown in RPMI media. All the complete growth mediums contained 10 % serum and 1% pen-strep (penicillin + streptomycin).

2.6.2 Biocompatibility Study using HDFa and HPV7 cells

To evaluate the cytotoxic effects of BSM-MNPs, these particles were incubated with HDFa and HPV7 cells. Briefly, 5000 cells/well were seeded in a 96 well plate and were allowed to attach for 24 hours. Further, varying concentrations (500 µg/ml, 300 µg/ml, 200 µg/ml, 100 µg/ml, 50 µg/ml and 0 µg/ml) of UV sterilized nanoparticles were suspended in respective growth mediums and were added to seeded cells followed by incubation for 24 hours. After 24 hours of exposure, the cell viability percentage was determined using colorimetric MTS assay (Cell Titer 96® Aqueous One Solution Cell Proliferation Assay, Promega), per manufacturer's instructions.

2.7 *In vitro* and *In vivo* Optical Imaging Capabilities

Based on results obtained from all particle characterizations for physicochemical, biological, and magneto-fluorescent properties, the best particle of studied BSM-MNPs was selected and used for further *in vitro* and *in vivo* studies. Particularly, fluorescence exhibited by these chosen particles was imaged *in vitro* and *in vivo*. For *in vitro* studies, PC3 cells were seeded in a 48 well plate and were allowed to attach for 24 hours. Particles were suspended in RPMI media and added on the cells followed

by 2 hours of incubation. Subsequent to 2 hour incubation, media was aspirated, and cells were washed with PBS extensively to get rid of extra particles not uptaken by cells. Cells were then fixed using 4% parafomaldehyde and were imaged for fluorescence under a fluorescent inverted microscope (Nikon) at 10X.

In vivo imaging was performed in agreement to the animal welfare policy with protocols approved by the University of Southwestern Medical Center at Dallas and University of Texas at Arlington. Initially, male nude mice, NOD SCID 6-8 weeks old, were anesthetized by supplying isoflurane gas, followed by subcutaneous inoculation of the tumor as previously described [43]. The tumor was then allowed to grow until it was palpable. Once the tumor had fully grown, particles were injected intra-tumorally with MNP-HA-BPLP and MNP-Click-BPLP particles as experimental groups and BPLP-MNPs as a control. Right after injection of particles, the mice were sacrificed by an overdose of CO_2 and were imaged for fluorescence under KODAK FX Pro imaging system (Carestream).

2.8 Therapeutic Studies

2.8.1 Uptake of Nanoparticles by Cancer Cells

As mentioned earlier, based on results obtained from physicochemical, biological, and magneto-fluorescent properties, the best one of the BSM-MNPs was chosen for further *in vitro* and *in vivo* studies. Cellular uptake study was conducted on all cancer cell lines. Briefly, cancer cells with a seeding density of 5000 cells/well were seeded on a 96 well plate. The seeded cells were allowed to attach for 24 hours, and then varying concentrations (500 µg/ml, 300 µg/ml, 200 µg/ml, 100 µg/ml, 50 µg/ml and 0 µg/ml) of UV sterilized nanoparticles were suspended in the respective growth mediums. The nanoparticle suspensions were then added onto the cells and followed by incubation for 2 hours. After 2 hours of exposure, cells were washed extensively to remove all extra nanoparticles, and 1X triton was added to each well to lyse the cells. The cell-lysate was used to quantify the amount of iron uptaken by cancer cells normalized with the total cell DNA using the iron and Pico green DNA assays (Invitrogen, CA), as described earlier.

2.8.2 Drug Release Study

Paclitaxel and docetaxel were chosen as the model anti-cancer drugs for the drug release study. Briefly, these drugs were encapsulated within nanoparticles during formation as described earlier, and drug release was performed for the duration of 21 days. 1mg of drug was added to the polymer solution by following protocol as described earlier for nanoparticle formation. Loading efficiency was calculated by an indirect method using formula.

$$\% \text{ Loading Efficiency} = \frac{\text{Amount of drug used} - \text{Amount of drug in supernatent}}{\text{Amount of drug used}} \times 100$$

For release studies, the drug loaded nanoparticles were suspended in DI water and incubated at 37^0C over a time range. At predetermined time points, the supernatant with released drug was collected and stored at -20^0C for later analysis. At the end of 21 days, all the samples containing paclitaxel and docetaxel were read using a U-Vis spectrophotometer at 235nm and 230nm, respectively, against standards to determine the drug contents and obtain the drug release curves.

2.8.3 Therapeutic effect of BSM-MNPs on Thyroid cancer cells

A preliminary study on therapeutic effects of anti-cancer drugs encapsulated within SMB-MNPs on thyroid cancer cells was investigated and compared with those of free drugs. The anti-cancer drug used for this study was paclitaxel (PAX). Free PAX and nanoparticles without drugs serve as positive and negative controls while drug loaded nanoparticles were used as the experimental group. Concentrations (50 µg/ml, 10 µg/ml, 1 µg/ml and 0 µg/ml) of free drugs and drugs within particles were chosen to be the same and amounts of particles without drugs were chosen to be the same as the amounts of drug-loaded nanoparticles. Briefly, thyroid cancer cells were seeded on a 96-wells plate with a seeding density of 5000 cells/well and were allowed to attach for 24 hours. Free drug and particles with and without drugs were then suspended in the media and added to cells followed by 24 hours incubation. To evaluate the

therapeutic effect of PAX loaded BSM-MNPs, cell viability was measured after 24 hours of exposure using MTS assays as described earlier.

CHAPTER 3

RESULTS AND DISCUSSION

3.1 Morphological & Functional Characteristics of BSM-MNPs

The table below describes the size, polydispersity and zeta potential values of the surface modified MNPs and BSM-MNPs. It can be clearly seen that particle size and zeta potential values of BSM-MNPs increased compared to the modified MNPs only (MNP-Si: 18 nm, -21mV and MNP-HA: 67 nm, -20.79 mV). The increased zeta potential values indicate the increased stability of particles [37]. The particle size of BSM-MNPs varied from 250 nm to 350 nm with MNP-Si-BPLP-BPLP and MNP-HA-BPLP about 290 nm and 280 nm, whereas MNP-Click-BPLP particles were about 335nm. Additionally, the polydispersity index of MNP-Si-BPLP-BPLP and MNP-HA-BPLP was well within the range (0.08-0.2) of well dispersed particle suspensions, except for MNP-Click-BPLP, which was 0.39 (Table 3.1). Zeta potential of all BSM-MNPs was also observed to be about -30 to -40, indicating particle stability and minimal aggregation. Thus, BSM-MNPs synthesized were highly stable with the particle size ranging from 250-350nm.

Table 3.1 Size distribution and zeta potential values of BSM-MNPs

Sample	Diameter (nm)	Polydispersity Index	Zeta Potential (mV)
MNP-Si	18	0.28	-21
MNP-HA	67	0.37	-20.79
MNP-Si-BPLP-BPLP	290	0.15	-40.20
MNP-HA-BPLP	280	0.26	-40.71
MNP-Click-BPLP	337	0.39	-33.63

The TEM images in Figure 3.1 confirm the spherical morphology of BSM-MNPs with the modified MNPs forming the core and polymer layer forming the shell. However, the particles size obtained from TEM was about 200 nm-250 nm for all BSM-MNPs, smaller than the sizes obtained using DLS. The difference in nanoparticle size determined by DLS and TEM can be attributed to the water absorption of nanoparticles as DLS measures nanoparticles in solution, causing an increase in the hydrodynamic diameter [44, 45].

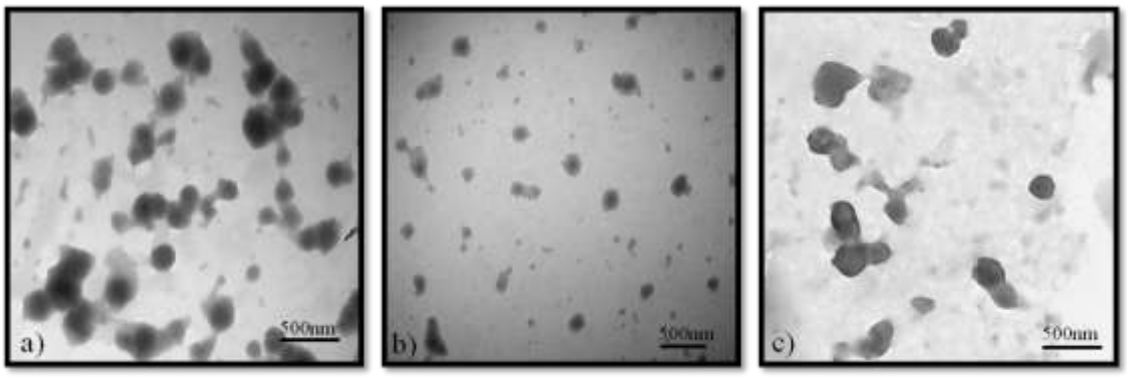

Figure 3.1 TEM images a) MNP-Si-BPLP-BPLP b) MNP-HA-BPLP c) MNP-Click-BPLP particles showing spherical morphology with core-shell orientation

To confirm the presence of all chemical structures from various coatings on BSM-MNPs, FTIR was conducted. As observed in Figure 3.2 (a), the peak at 2919 cm^{-1} corresponding to –CH2 group (polymer backbone) is visible in FTIR spectra for all particles. Similarly, characteristic peaks of -C=O from citric acid at 1707 cm^{-1} and –C (=O) NH between polymer and amino acid at 1550 cm^{-1} [33]. Also, the characteristic peaks of carbonate at 1300-1600 cm^{-1}, phosphate at 1190-976 cm^{-1} and hydroxyl stretch at 3570 cm^{-1} corresponding to presence of Hydroxypatite coating on MNPs [46]. Thus the FTIR spectra for all the samples confirmed the presence of all the chemical bonds from the polymer and MNP surface coatings.

BSM-MNPs were also characterized for their stability in media containing serum over a period of 7 days. The particles were observed to be stable over a period of 7 days without any aggregation (an

increase in particle size would indicate particle aggregation) as shown in Figure 3.2 (b). The decrease in particle size with time might be due to the degradation of these nanoparticles. A similar trend was observed with polydispersity index (Figure 3.2 (c)). It is also observed that MNP-HA-BPLP particles maintained their hydrodynamic diameters in both DI water and media.

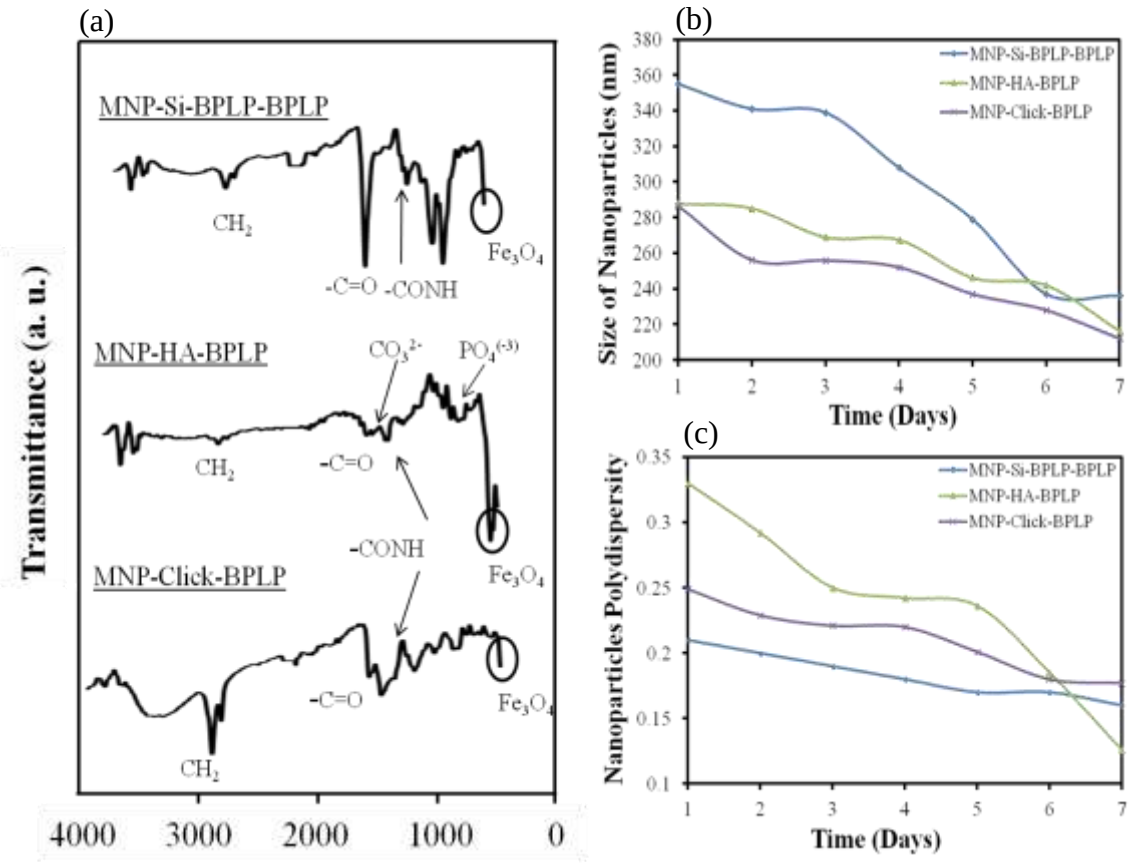

Figure 3.2 (a) FTIR Spectrum of MNP-Si-BPLP-BPLP, MNP-HA-BPLP and MNP-Click-BPLP particles showing characteristic peaks for all chemical bonds, Stability study showing (b) Decreasing particle size (c) Decreasing polydispersity index over a period of 7 days

3.2 Magnetic Targeting Capability

The iron content presented in SMB-MNPs was evaluated by performing iron assays on these particles. As shown in Figure 3.3 (a), MNP-HA-BPLP and MNP-Click BPLP particles contain a maximum iron content of 87% and 86%, respectively, whereas MNP-Si-BPLP-BPLP show a slightly lower iron content of 79%. The lesser iron mass presented in MNP-Si-BPLP-BPLP can be attributed to two polymer coatings on MNPs thus containing more polymer when compared to the same weight amount of MNP-HA-BPLP and MNP-Click-BPLP particles.

The evaluation of iron mass content was followed by the measurement of magnetization values of BSM-MNPs. As observed in Figure 3.3 (b), bare magnetic nanoparticles exhibit maximum magnetization of 60emu/g. Similarly, MNP-Si-BPLP-BPLP, MNP-Click-BPLP maintain about the same magnetization value as the original MNPs. However, MNP-HA-BPLP has reduced magnetization values compared to other particles. The reduction in the magnetization is attributed to the HA coating, which may be responsible for producing a delayed response to the magnetic field applied. Nonetheless, MNP-HA-BPLP nanoparticles exhibit the hysteresis loop, indicating that particles possess superparamagnetic properties. Further, all experimental group particles possess a magnetization value superior to 20emu/g (Figure 3.3(b)), indicating superparamagnetic behavior of all the particles.

(a)

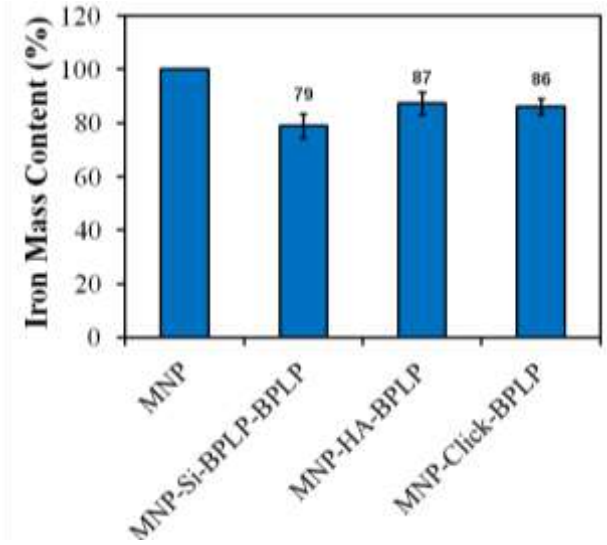

(b)

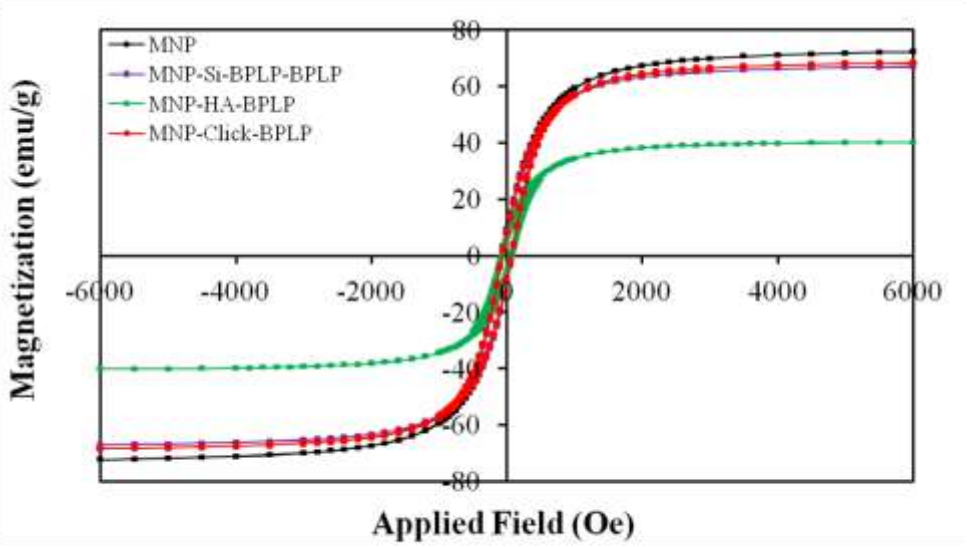

(c)

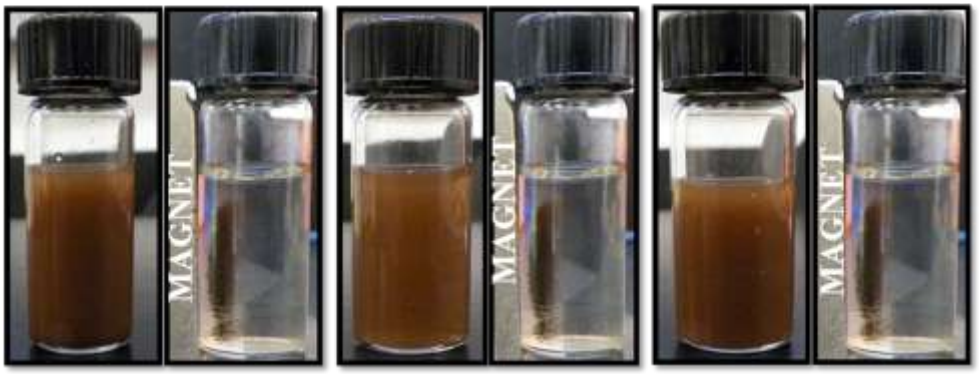

MNP-Si-BPLP-BPLP MNP-HA-BPLP MNP-Click-BPLP

Figure 3.3 Represents (a) %Iron mass content (b) Hysteresis loop for magnetization values (c) Images of MNP-SI-BPLP-BPLP, MNP-HA-BPLP and MNP-Click-BPLP particles indicating nanoparticles suspension on the left whereas showing recruitment of nanoparticles under the influence of magnetic field (1.3 T)

Lastly, magnetic targeting of SMB-MNPs was also demonstrated by recruiting MNPs under the influence of external magnetic field. As seen in Figure 3.3 (c) images, the left tubes represent a highly dispersed MNP solution in the absence of a magnetic field; however, upon application of a magnetic field, these nanoparticles are recruited in the direction of a magnetic field as seen in the right tubes. The

magnetic targeting results from the above studies suggest that BSM-MNPs possess superparamagnetic properties and magnetic targeting abilities despite the surface modifications and polymer coatings.

3.3 Diagnostic Capabilities of BSM-MNPs

MR imaging was performed to assess whether these modified nanoparticles could serve as the MRI contrast reagent. Figure 3.4 (a) represents the MRI image of only agarose gel sample demonstrating no contrast, whereas Figure 3.4 (d) shows an MRI image of bare MNPs, demonstrating darkest contrast. Further, Figure 3.4 (b) and (c) represent MRI of the polymer BPLP and Click-BPLP, respectively, showing no contrast at all. The MNP-Click-BPLP (g) and MNP-HA-BPLP (f) particles exhibit darkest contrast, which is comparable to the contrast produced by bare MNPs. MNP-Si-BPLP-BPLP (e) expressed lighter contrast in comparison to other experimental groups. The MRI results are in unison to the iron content presented in all the surface modified nanoparticles as seen in Figure 3.3 (a). Additionally, the percentile drop in MRI signal intensity was quantified and it was observed that bare MNPs and MNP-Click-BPLP particles have comparable values of 54.61 % and 48.02 %, respectively. However, minimal intensity drop was observed from MNP-Si-BPLP-BPLP particles (17.11 %) and MNP-HA-BPLP particles (44.47 %).

In order to evaluate the optical imaging properties of BSM-MNPs, cytoviva imaging and emission spectra were performed. As seen in Figure 3.5 images (a), (b), and (c) exhibit improved fluorescence from BSM-MNPs compared to the previously developed BPLP-MNPs in image (d). The superior fluorescence can be attributed to the surface modifications of MNPs to cover the blackness of MNPs. However, fluorescence seen in images (b) and (c) is superior to fluorescence in images (a), as HA imparts lighter color for MNPs and click chemistry directly conjugates polymer onto MNPs (end-grafted polymer coating), whereas Si functionalization provides a transparent coat onto MNPs, thereby not covering the blackness of MNPs completely. Additionally, MNP-Si-BPLP-BPLP nanoparticles have improved fluorescence compared to BPLP-MNPs due to the dual polymer layer coating on MNP-Si. In

conclusion, all the surface modifications performed on MNPs provide improved fluorescence compared to that without surface modification, BPLP-MNPs.

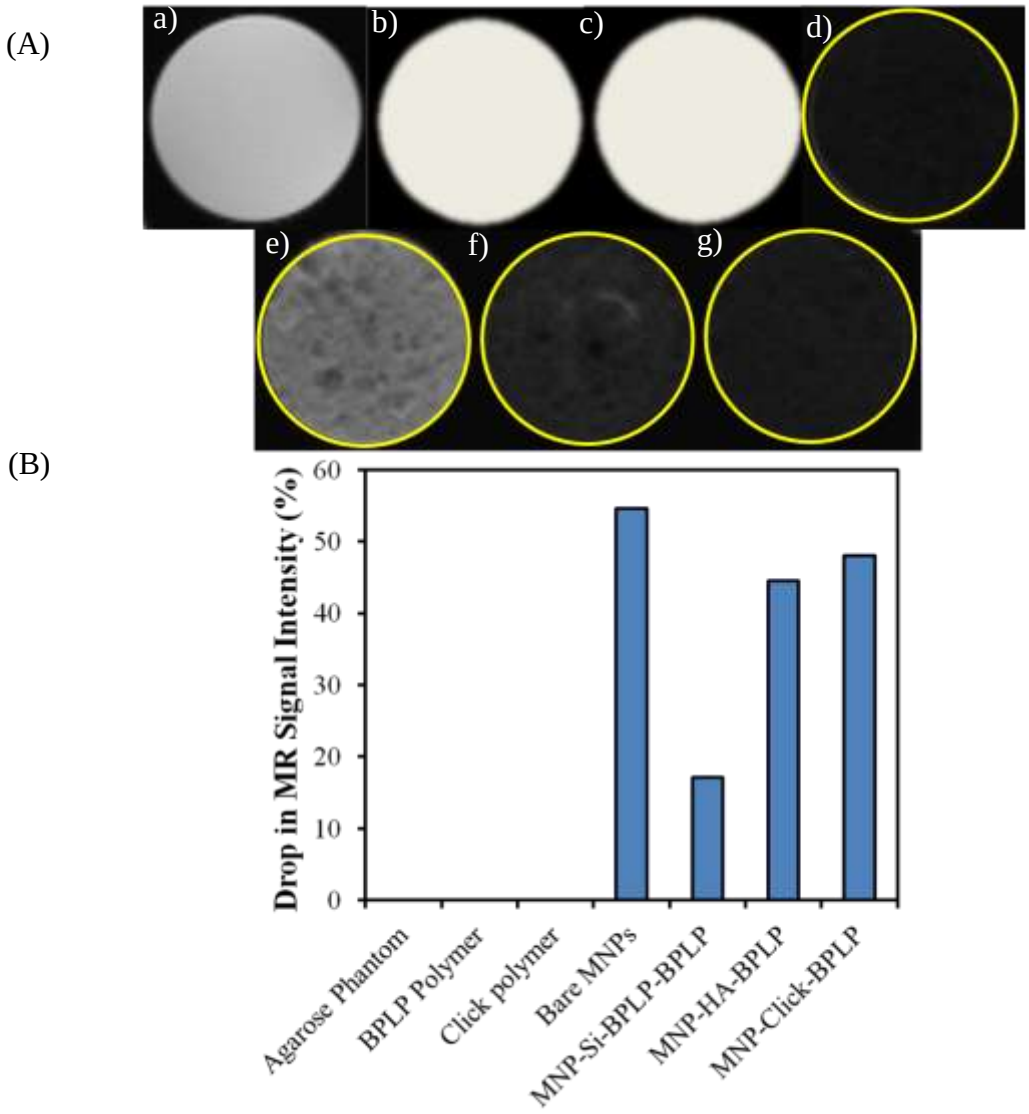

Figure 3.4 (A) MR images of agarose phantoms containing (a) Agarose phantom (b) BPLP polymer (c) Click-BPLP polymer (d) Bare MNPs (e) MNP-Si-BPLP-BPLP particles (f) MNP-HA-BPLP particles (g) MNP-Click-BPLP particles (B) Represents the % intensity drop in MR signal from experimental group BSM-MNPs in comparison to the control groups

Furthermore, emission spectra performed for BSM-MNPs confirmed the increased fluorescence intensity compared to BPLP-MNPs. As observed in Figure 3.6, MNP-Click-BPLP particles exhibit the highest fluorescence intensity followed by MNP-HA-BPLP particles, and lastly MNP-Si-BPLP-BPLP particles. Additionally, a red shift is observed with MNP-HA-BPLP particles, as the emission peak wavelength has shifted towards the red region when compared to MNP-Si-BPLP-BPLP and MNP-Click-BPLP. The red-shifting of the emission peak may be useful for imaging as it would reduce the effects of autofluorescence [48].

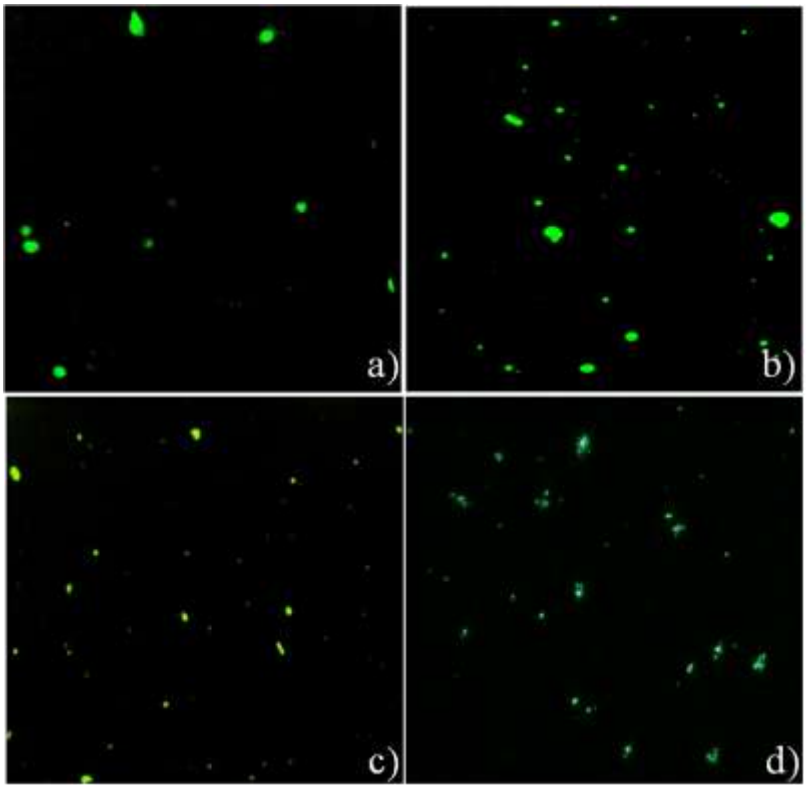

Figure 3.5 Cytoviva images demonstrating fluorescence from (a) MNP-Si-BPLP-BPLP (b) MNP-HA-BPLP (c) MNP-Click-BPLP (d) BPLP-MNPs

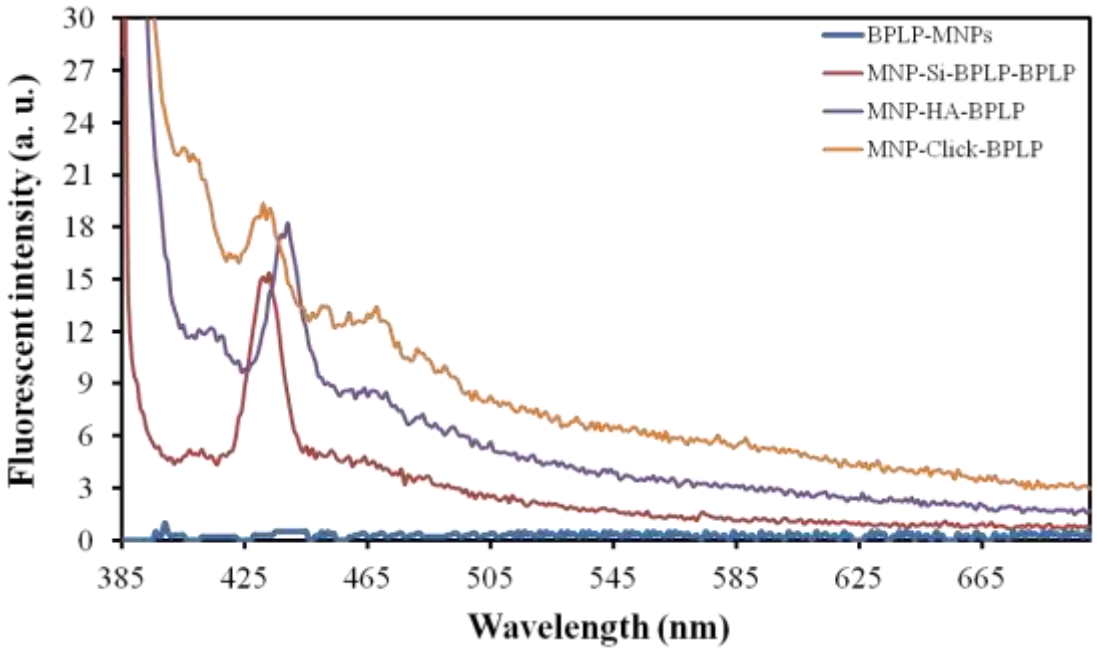

Figure 3.6 Emission spectra of BSM-MNPs at a constant excitation wavelength of 375 nm for MNP-SI-BPLP-BPLP and MNP-HA-BPLP particles, and 360 nm for MNP-Click-BPLP particles

3.4 HDFa and PZ-HPV-7 Cell Viability Study

The toxicity of particles was evaluated on both HDFs and PZ-HPV-7 cells. Figure 3.7 (a) below describes the toxicity trend of all experimental particles on HDF cells as a measurement of the percentage of cell viability. It can be seen that all surface modified BPLP-MNPs were highly biocompatible up to a concentration of 300µg/ml, however, the percentage of cell viability of HDFs decreased significantly with increasing concentrations. At concentrations above 300µg/ml, these nanoparticles showed significant cell death in comparison to control samples (without particle exposure). Further, as shown in Figure 3.7 (b), it can be seen that all particles are biocompatible up to 300 µg/ml concentration using PZ-HPV-7. Unlike MNP-Si-BPLP-BPLP, MNP-HA-BPLP and MNP-Click-BPLP particles shows significant cell death with cell viability less than 80% when normal prostate cells (PZ-HPV-7) were exposed to these nanoparticles at 500 µg/ml concentrations.

By taking into consideration the results obtained from all studies, it can be concluded that MNP-HA-BPLP and MNP-Click BPLP have comparable stability, biocompatibility, and magnetic and imaging properties. Therefore, due to these these superior properties, MNP-HA-BPLP and MNP-Click-BPLP particles were chosen for further *in vitro* and *in vivo* optical imaging.

3.5 Enhanced Optical Imaging Properties *in vitro* and *in vivo*

MNP-HA-BPLP and MNP-Click-BPLP particles were further evaluated *in vitro* and *in vivo* for optical imaging capabilities using cell cultures such as prostate cancer cell line (PC3 cells) and animal models (nude mice). Primarily, cellular imaging was performed with MNP-HA-BPLP and MNP-Click-BPLP particles on PC3 cells. As observed in Figure 3.8 (a) PC3 cells with BPLP-MNPs possess less fluorescence intensity. However, PC3 cells exposed to MNP-HA-BPLP (b) and MNP-Click-BPLP (c) particles exhibit excellent fluorescence compared to BPLP-MNPs. Additionally, all the cells seen in the image are fluorescently labeled by both MNP-HA-BPLP and MNP-Click-BPLP particles thus proving the efficiency of optical imaging. PC3 cells with MNP-HA-BPLP particles also show excellent fluorescence signals compared to MNP-Click-BPLP particles as observed in Figure 3.8.

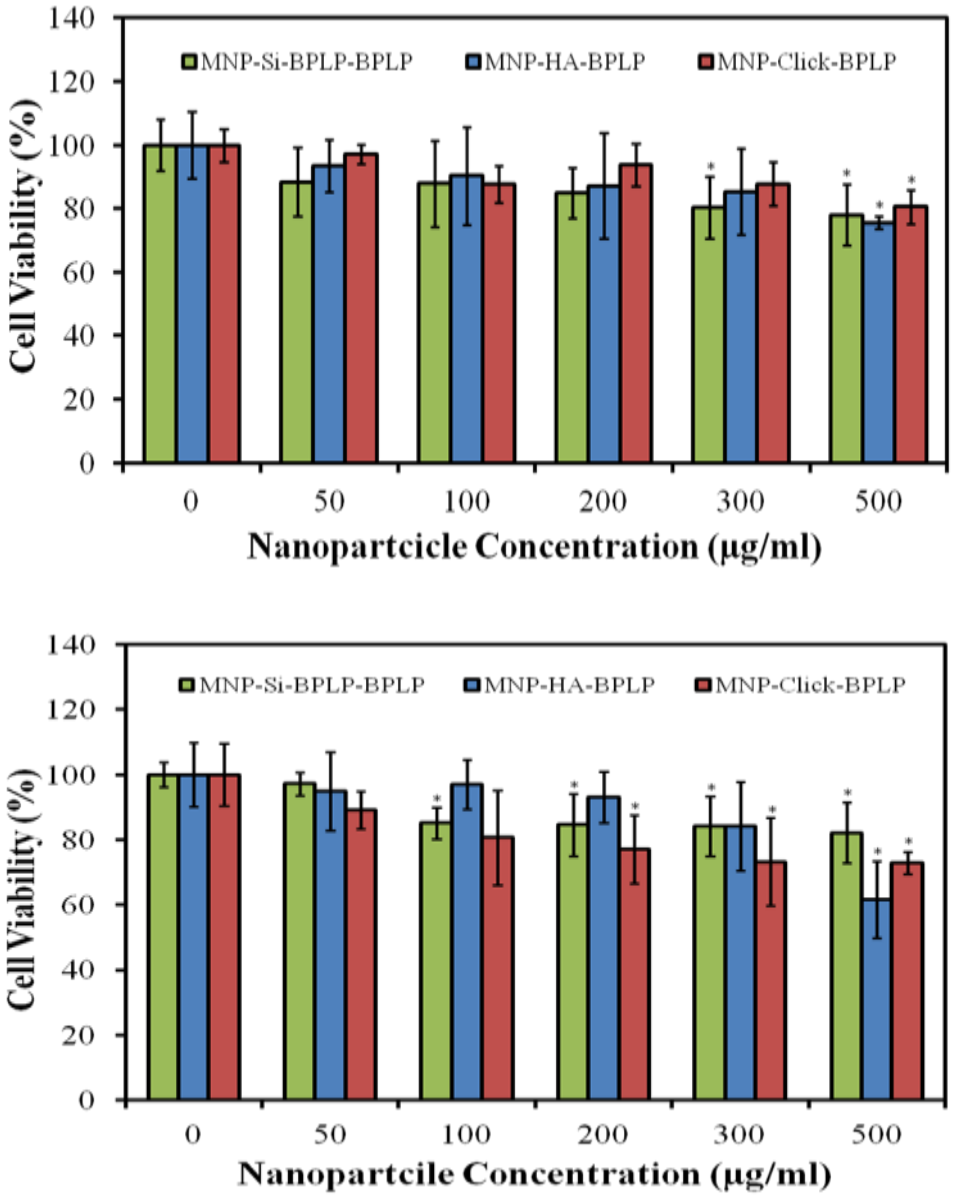

Figure 3.7 Biocompatibility Studies of SMB-MNPs with (a) HDFa cells and (b) HPV7 cells showing excellent biocompatibility up to 300 µg/ml concentration after 24 hours of exposure to BSM-MNPs with a significant difference of $p < 0.05$

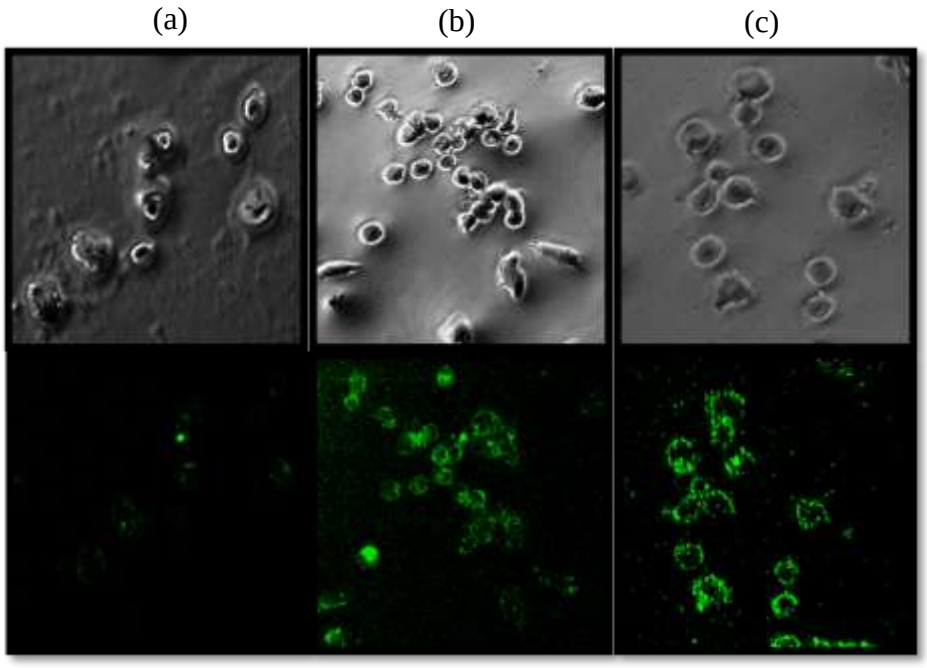

Figure 3.8 *In vitro* fluorescent images (a) PC3 cells with BPLP-MNPs (b) PC3 cells with MNP-HA-BPLP particles, and (c) PC3 cells with MNP-Click-BPLP particles; above image representing the monochrome image and FITC image below

In vivo results also confirmed that the fluorescence signal exhibited by MNP-HA-BPLP particles was more compared to those of MNP-Click-BPLP and BPLP-MNPs. As observed in Figure 3.9 (A) (a), no fluorescence is visible in the tumor region of control animals, whereas in images (b) BPLP-MNPs and (c) MNP-Click-BPLP, the fluorescence is comparable to each other. Conversely, Figure 3.9 image (d) demonstrates that the tumor using MNP-HA-BPLP particles exhibits excellent fluorescence in comparison to both BPLP-MNPs and BPLP-Click-MNPs, suggesting MNP-HA-BPLP possesses better optical imaging properties. As seen in Figure 3.9 (b) the fluorescence intensity of *in vivo* images calculated also suggests that MNP-HA-BPLP particles possess the highest fluorescence intensity in comparison to both MNP-Click-BPLP particles and BPLP-MNPs.

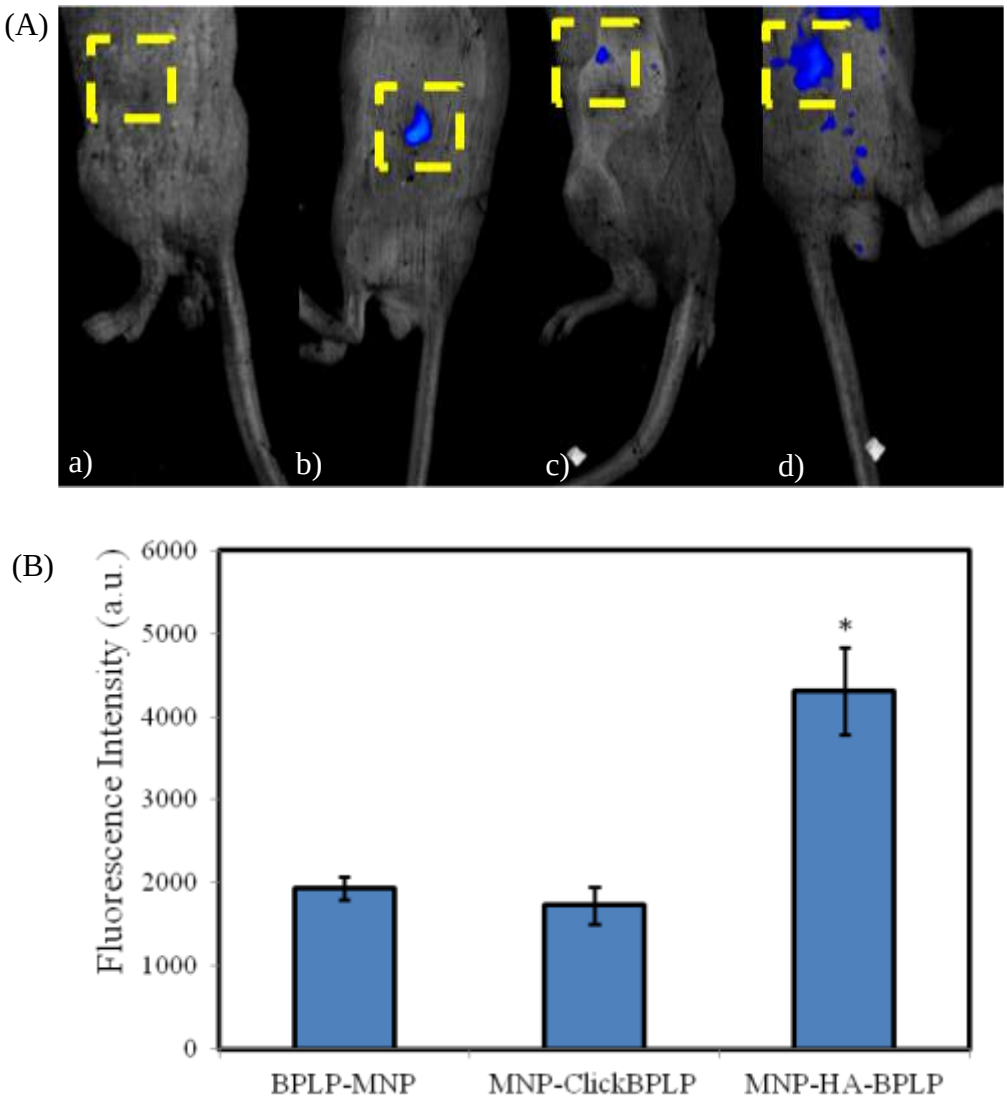

Figure 3.9 (A) In vivo images showing fluorescence from (a) tumor only (b) BPLP-MNPs (c) MNP-Click-BPLP particles (d) MNP-HA-BPLP particles (B) Fluorescence intensity of *in vivo* imaging

3.6 Therapeutic Capabilities of BSM-MNPs

3.6.1 Uptake Efficiency of BSM-MNPs by cancer cells

Cellular uptake as observed in Figure 3.10 (a) was dose-dependent and increased with increasing concentrations for both TT cells and KAT-4 (Thyroid cancer cell lines). It can be clearly seen that at a concentration up to 100µg/ml, there is a considerably lower uptake; however, as the concentration was

increased, higher uptake was observed, indicating the dose-dependent trend. Furthermore, it can be seen that the uptake by KAT-4 cells is higher than TT cells. A similar dose-dependent trend was also observed in PC3 and LNCaP prostate cancer cells as shown in Figure 3.10 (b). Moreover, LNCaP was observed to have a higher uptake in comparison to PC3 cells. Uptake of MNP-HA-BPLP particles by G361 skin cancer cells (Figure 3.10 (c)) was also dose-dependent. The dose-dependent nature of uptake may be useful in delivering higher amounts of therapeutic agents.

3.6.2 Drug Release Profile

The drug release study involved the use of two drugs, namely Docetaxel and Paclitaxel, with a loading efficiency of 68% and 71%, respectively. There was not much of a difference between the loading efficiencies of both the drugs, specifying that about 70% of the drug can be loaded in MNP-HA-BPLP particles. The drug release profiles shown in Figure 3.11 demonstrate that about 82.3% paclitaxel was released over a period of 21 days with an initial burst release over a period of 48 hours. Docetaxel also showed a similar trend, with 79.8% drug release over 21 days. The loading efficiencies and drug release profiles of both drugs showed similar trends, indicating the ability of BPLP polymer to degrade and deliver almost all of the drug loaded over a period of 21 days, to provide a sustained drug release for drug delivery applications.

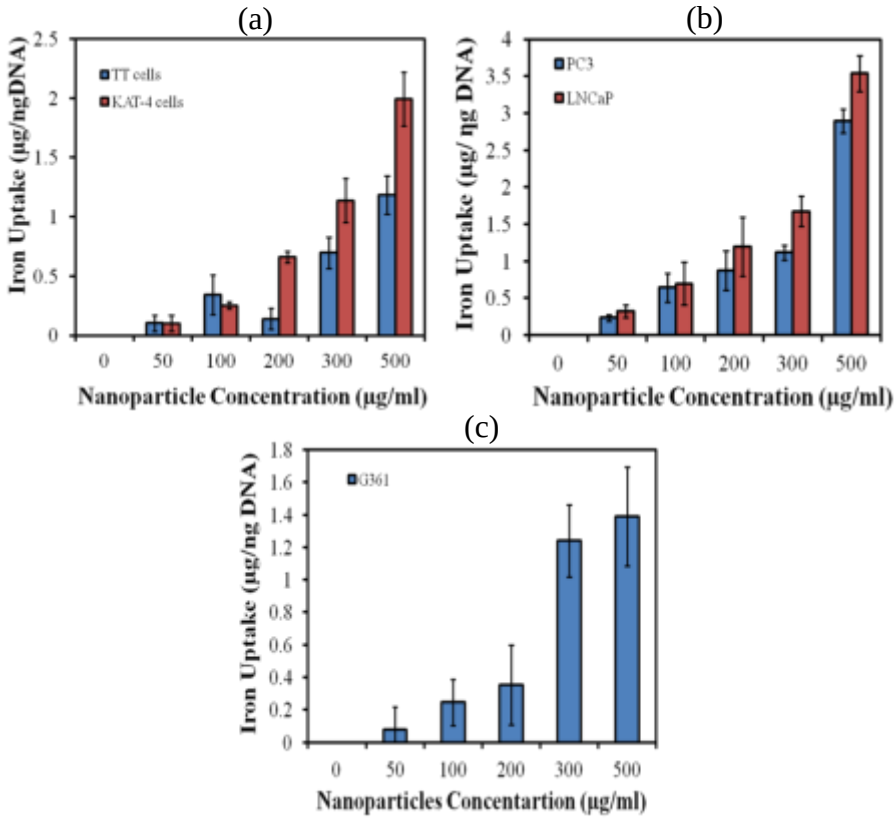

Figure 3.10 Cellular uptake of MNP-HA-BPLP particles a) thyroid cancer cell lines b) Prostate cancer cell lines, and c) Skin cancer cell lines showing dose dependent uptake

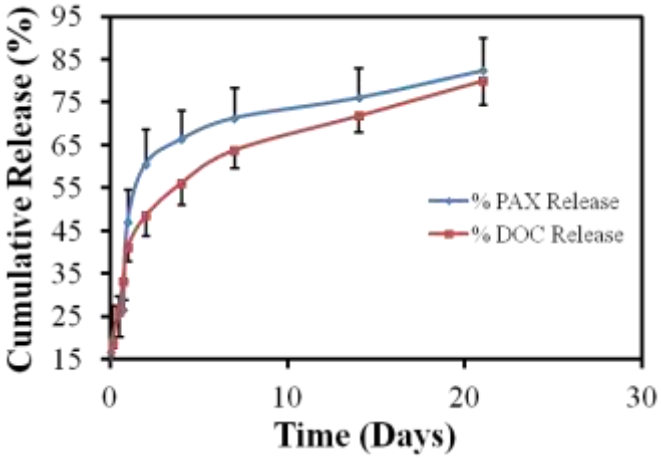

Figure 3.11 Drug release profiles showing 82% release of Paxclitaxel and 79% release of Docetaxel over a period of 21 days

3.6.3 Efficiency of BSM-MNPs-Drug Formulation on Cancer Cell Viability

To determine the efficiency of SMB-MNPs as a drug carrier for cancer therapy, the effect of free paclitaxel amounts on cell survival was compared to the same amounts of drug released from particles at predetermined time points. As observed in Figure 3.12 (A) with an increasing concentration of free drug, cell survival decreased when KAT-4 thyroid cancer cells were used. Similarly, the cell viability due to drug loaded MNP-HA-BPLP particles also decreased significantly, thus indicating the therapeutic efficiency of particles. Moreover, a similar trend was observed in the percentage cell viability of TT cells between free PAX and PAX-loaded MNP-HA-BPLP particles. MNP-HA-BPLP particles only did not affect the cell viability significantly. These results signify that drug loaded MNP-HA-BPLP particles can deliver similar effects as the free drug. Thus the systemic toxicity can be avoided by delivering drug loaded BSM-MNPs at the target site with the help of magnetic targeting.

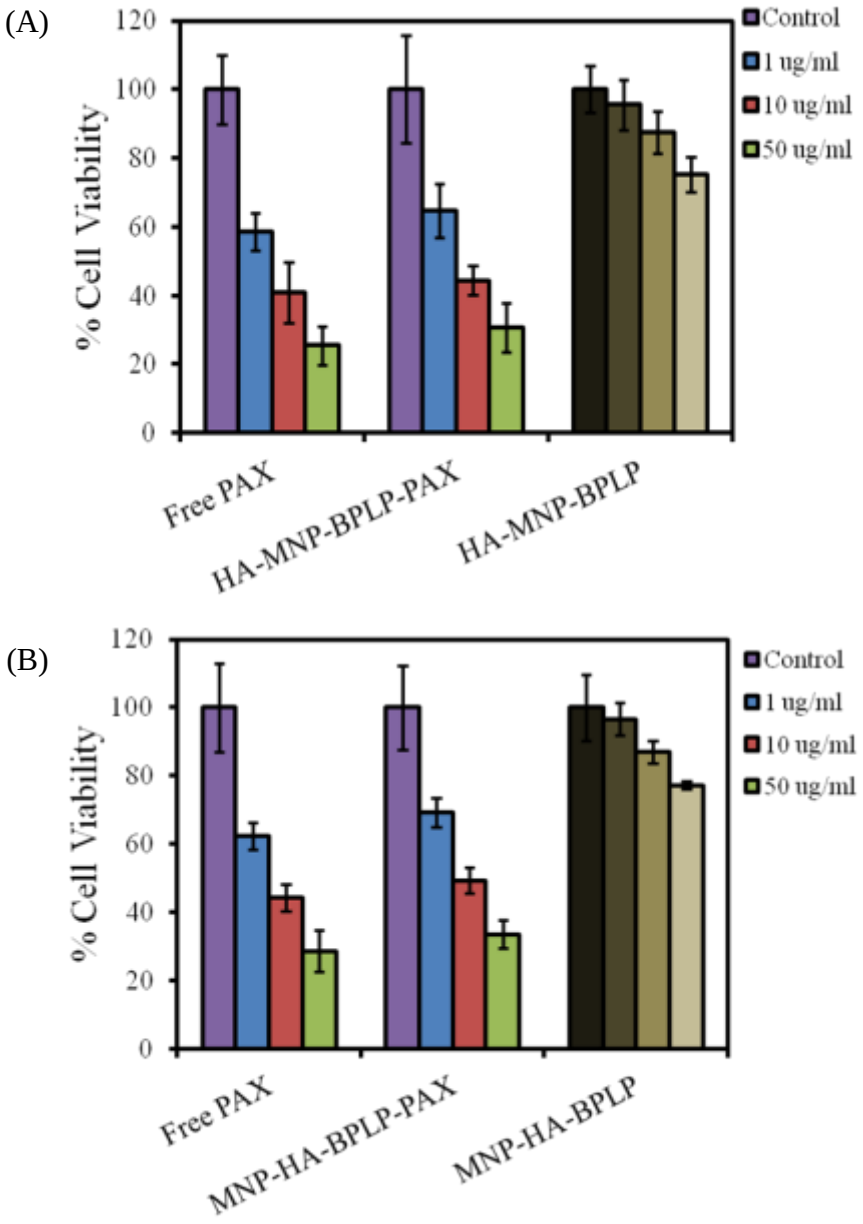

Figure 3.12 Therapeutic Effect of Drug loaded MNP-HA-BPLP on (A) KAT-4 thyroid cancer cells (B) TT-thyroid cancer cells showing similar effect in cell death between free drug and drug encapsulated MNP-HA-BPLP particles

CHAPTER 4

SUMMARY

4.1 Conclusion

This research work aimed at applying various surface modifications on MNPs to cover their blackness and enhance the fluorescence of BPLP-coated MNPs for better *in vivo* imaging applications. Various surface modifications such as Silane (Si), Hydroxypatite (HA), and Si-Azide were adopted to achieve this goal. The BSM-MNPs developed were then characterized for physicochemical and magneto-fluorescent properties followed by the evaluation of biocompatibility. The polymer-coated surface-modified MNPs were stable and possessed core-shell structures with a diameter ranging from 200nm–350nm. Additionally, BSM-MNPs had excellent magneto-fluorescent properties over previously developed BPLP-MNPs, with MNP-HA-BPLP and MNP-Click-BPLP particles having exceptional optical imaging capabilities. The fluorescence of MNP-HA-BPLP and MNP-Click-BPLP particles evaluated *in vitro* and *in vivo* showed that MNP-HA-BPLP particles exhibit maximum fluorescence intensity compared to BPLP-MNPs and MNP-Click-BPLP particles. Thus the first aim to enhance fluorescence from BPLP-MNPs by surface modification of MNPs was successfully achieved.

Further, SMB-MNPs developed were highly biocompatible and possessed high efficacy of being uptaken by cancer cells in a dose dependent manner. Additionally, MNP-HA-BPLP particles were able to deliver about 80% drug loaded over a period of 21 days. The trend of dose-dependent uptake by cancer cells and the ability to deliver drugs over a time range suggests the potential of MNP-HA-BPLP as an effective therapy. Moreover, BPLP is completely biodegradable; therefore, it will be cleared out of the system completely, whereas hydroxypatite is an element present in the bones, proving to be harmless. Thus the system MNP-HA-BPLP consists of biocompatibility, excellent magnetic targeting, and dual imaging capabilities while providing good therapeutic effects, and proving them to be suitable theranostic particles for cancer management.

4.2 Limitations and Future Work

Limitations of this research include:

- The use of Superparamagnetic nanoparticles that have recently been withdrawn from the market by the FDA. This limitation can be certainly overcome by the use of FDA approved Gadolinium based MRI agents which are still on the market for human use.
- The size of BSM-MNPs is above 200 nm which might be uptaken by macrophages and cleared by RES. This limitation can be conquered by either filtering the particles with 0.2 μm filter or adjusting the surfactant amounts during the particle formulation process.
- The fluorescent signals of these particles are reduced with the penetration depth, thus they are applicable to superficial tumors only.

Future Work should be considered to:

- Evaluate therapeutic effects of drug-loaded MNP-HA-BPLP particles on both prostate and skin cancer cell lines.
- Study the magnetic targeting efficiency of particles *in vivo*.
- Investigate *in vivo* therapeutic effects of MNP-HA-BPLP particles loaded with anti-cancer drugs on tumor size reduction.
- Determine the effectiveness of MNP-HA-BPLP nanoparticles as theranostic nanoparticles to detect and treat cancers *in vivo*.

REFERENCES

[1] DelSal G, Loda M, Pagano M. Cell cycle and cancer: critical events at the G1 restriction point. Critical reviews in oncogenesis. 1996;7(1-2):127-42.

[2] Martinez JC, Otley CC, Stasko T, Euvrard S, Brown C, Schanbacher CF, et al. Defining the clinical course of metastatic skin cancer in organ transplant recipients: a multicenter collaborative study. Archives of dermatology. 2003 Mar;139(3):301-6.

[3] Pienta KJ, Naik H, Akhtar A, Yamazaki K, Replogle TS, Lehr J, et al. Inhibition of spontaneous metastasis in a rat prostate cancer model by oral administration of modified citrus pectin. Journal of the National Cancer Institute. 1995 Mar 1;87(5):348-53.

[4] Silverberg SG, Hutter RV, Foote FW, Jr. Fatal carcinoma of the thyroid: histology, metastases, and causes of death. Cancer. 1970 Apr;25(4):792-802.

[5] Yoo D, Lee JH, Shin TH, Cheon J. Theranostic magnetic nanoparticles. Accounts of chemical research. Oct 18;44(10):863-74.

[6] Yezhelyev MV, Gao X, Xing Y, Al-Hajj A, Nie S, O'Regan RM. Emerging use of nanoparticles in diagnosis and treatment of breast cancer. The lancet oncology. 2006 Aug;7(8):657-67.

[7] Bardhan R, Lal S, Joshi A, Halas NJ. Theranostic nanoshells: from probe design to imaging and treatment of cancer. Accounts of chemical research. Oct 18;44(10):936-46.

[8] Ma X, Zhao Y, Liang XJ. Theranostic nanoparticles engineered for clinic and pharmaceutics. Accounts of chemical research. Oct 18;44(10):1114-22.

[9] Xiao Z, Levy-Nissenbaum E, Alexis F, Luptak A, Teply BA, Chan JM, et al. Engineering of targeted nanoparticles for cancer therapy using internalizing aptamers isolated by cell-uptake selection. ACS nano. Jan 24;6(1):696-704.

[10] Dekiwadia CD, Lawrie AC, Fecondo JV. Peptide-mediated cell penetration and targeted delivery of gold nanoparticles into lysosomes. J Pept Sci. Jul 4.

[11] Taheri A, Dinarvand R, Ahadi F, Khorramizadeh MR, Atyabi F. The in vivo antitumor activity of LHRH targeted methotrexate-human serum albumin nanoparticles in 4T1 tumor-bearing Balb/c mice. International journal of pharmaceutics. Jul 15;431(1-2):183-9.

[12] Wang Y, Li B, Xu F, Jia D, Feng Y, Zhou Y. In Vitro Cell Uptake of Biocompatible Magnetite/Chitosan Nanoparticles with High Magnetization: A Single-Step Synthesis Approach for In-Situ-Modified Magnetite by Amino Groups of Chitosan. Journal of biomaterials science. Mar 18.

[13] Banerjee SS, Chen DH. Cyclodextrin conjugated magnetic colloidal nanoparticles as a nanocarrier for targeted anticancer drug delivery. Nanotechnology. 2008 Jul 2;19(26):265602.

[14] Singh A, Dilnawaz F, Mewar S, Sharma U, Jagannathan NR, Sahoo SK. Composite polymeric magnetic nanoparticles for co-delivery of hydrophobic and hydrophilic anticancer drugs and MRI imaging for cancer therapy. ACS applied materials & interfaces. Mar;3(3):842-56.

[15] Heebeom Koo† MSH, In-Cheol Sun†, Soon Hong Yuk‡, Kuiwon Choi†, Kwangmeyung Kim*†, and Ick Chan Kwon*†. In Vivo Targeted Delivery of Nanoparticles for Theranosis. Accounts of chemical research. 2011 january 20;44(10):1018-28.

[16] Medina C, Santos-Martinez MJ, Radomski A, Corrigan OI, Radomski MW. Nanoparticles: pharmacological and toxicological significance. British journal of pharmacology. 2007 Mar;150(5):552-8.

[17] Tanner P, Baumann P, Enea R, Onaca O, Palivan C, Meier W. Polymeric vesicles: from drug carriers to nanoreactors and artificial organelles. Accounts of chemical research. Oct 18;44(10):1039-49.

[18] Immordino ML, Dosio F, Cattel L. Stealth liposomes: review of the basic science, rationale, and clinical applications, existing and potential. International journal of nanomedicine. 2006;1(3):297-315.

[19] Sun C, Lee JS, Zhang M. Magnetic nanoparticles in MR imaging and drug delivery. Advanced drug delivery reviews. 2008 Aug 17;60(11):1252-65.

[20] Xie J, Lee S, Chen X. Nanoparticle-based theranostic agents. Advanced drug delivery reviews. Aug 30;62(11):1064-79.

[21] Ng KK, Lovell JF, Zheng G. Lipoprotein-inspired nanoparticles for cancer theranostics. Accounts of chemical research. Oct 18;44(10):1105-13.

[22] Nie S, Xing Y, Kim GJ, Simons JW. Nanotechnology applications in cancer. Annual review of biomedical engineering. 2007;9:257-88.

[23] Danhier F, Feron O, Preat V. To exploit the tumor microenvironment: Passive and active tumor targeting of nanocarriers for anti-cancer drug delivery. J Control Release. Dec 1;148(2):135-46.

[24] Maeda H, Wu J, Sawa T, Matsumura Y, Hori K. Tumor vascular permeability and the EPR effect in macromolecular therapeutics: a review. J Control Release. 2000 Mar 1;65(1-2):271-84.

[25] Bonnemain B. Superparamagnetic agents in magnetic resonance imaging: physicochemical characteristics and clinical applications. A review. Journal of drug targeting. 1998;6(3):167-74.

[26] Lammers T, Aime S, Hennink WE, Storm G, Kiessling F. Theranostic Nanomedicine. Accounts of chemical research. 2011 2012/07/11;44(10):1029-38.

[27] Cabral H, Nishiyama N, Kataoka K. Supramolecular nanodevices: from design validation to theranostic nanomedicine. Accounts of chemical research. Oct 18;44(10):999-1008.

[28] Puech P, Huglo D, Petyt G, Lemaitre L, Villers A. Imaging of organ-confined prostate cancer: functional ultrasound, MRI and PET/computed tomography. Current opinion in urology. 2009 Mar;19(2):168-76.

[29] Choy G, Choyke P, Libutti SK. Current advances in molecular imaging: noninvasive in vivo bioluminescent and fluorescent optical imaging in cancer research. Molecular imaging. 2003 Oct;2(4):303-12.

[30] Wu X, Liu H, Liu J, Haley KN, Treadway JA, Larson JP, et al. Immunofluorescent labeling of cancer marker Her2 and other cellular targets with semiconductor quantum dots. Nat Biotech. 2003;21(1):41-6.

[31] Santra S, Kaittanis C, Grimm J, Perez JM. Drug/dye-loaded, multifunctional iron oxide nanoparticles for combined targeted cancer therapy and dual optical/magnetic resonance imaging. Small (Weinheim an der Bergstrasse, Germany). 2009 Aug 17;5(16):1862-8.

[32] Yang P, Quan Z, Hou Z, Li C, Kang X, Cheng Z, et al. A magnetic, luminescent and mesoporous core-shell structured composite material as drug carrier. Biomaterials. 2009 Sep;30(27):4786-95.

[33] Jian Yanga b, 1, Yi Zhanga,b, Santosh Gautama,b, Li Liuc, Jagannath Deya,b, Wei Chend, Ralph P. Masonb,c,, Carlos A. Serranoe KAS, and Liping Tanga,b. Development of aliphatic biodegradable photoluminescent polymers. PNAS. 2009;106(25):10086-91.

[34] Curtis CCBaASG. Functionalisation of magneticnanoparticles for applications inbiomedicine. TOPICAL REVIEW. 2003.

[35] Ste´phane Mornet SbV, Fabien Grasset and Etienne Duguet. Magnetic nanoparticle design for medical diagnosis and therapy. Journal of Materials Chemistry. 2004.

[36] Chen Y, Chen BA. [Application and advancement of magnetic iron-oxide nanoparticles in tumor-targeted therapy]. Chinese journal of cancer. Jan;29(1):125-8.

[37] Wadajkar AS, Kadapure T, Zhang Y, Cui W, Nguyen KT, Yang J. Dual-Imaging Enabled Cancer-Targeting Nanoparticles. Advanced Healthcare Materials.1(4):450-6.

[38] Rahimi M, Yousef M, Cheng Y, Meletis EI, Eberhart RC, Nguyen K. Formulation and characterization of a covalently coated magnetic nanogel. Journal of nanoscience and nanotechnology. 2009 Jul;9(7):4128-34.

[39] Koppolu B, Rahimi M, Nattama S, Wadajkar A, Nguyen KT. Development of multiple-layer polymeric particles for targeted and controlled drug delivery. Nanomedicine. Apr;6(2):355-61.

[40] Tran N, Webster TJ. Increased osteoblast functions in the presence of hydroxyapatite-coated iron oxide nanoparticles. Acta biomaterialia. Mar;7(3):1298-306.

[41] Schlossbauer A, Schaffert D, Kecht J, Wagner E, Bein T. Click chemistry for high-density biofunctionalization of mesoporous silica. Journal of the American Chemical Society. 2008 Sep 24;130(38):12558-9.

[42] Kim J, Lee JE, Lee J, Yu JH, Kim BC, An K, et al. Magnetic fluorescent delivery vehicle using uniform mesoporous silica spheres embedded with monodisperse magnetic and semiconductor nanocrystals. Journal of the American Chemical Society. 2006 Jan 25;128(3):688-9.

[43] Okegawa T, Li Y, Pong RC, Bergelson JM, Zhou J, Hsieh JT. The dual impact of coxsackie and adenovirus receptor expression on human prostate cancer gene therapy. Cancer research. 2000 Sep 15;60(18):5031-6.

[44] Lin JJ, Chen JS, Huang SJ, Ko JH, Wang YM, Chen TL, et al. Folic acid-Pluronic F127 magnetic nanoparticle clusters for combined targeting, diagnosis, and therapy applications. Biomaterials. 2009 Oct;30(28):5114-24.

[45] Shan L. Poly(N,N-dimethylacrylamide)-coated maghemite nanoparticles for labeling and tracking mesenchymal stem cells. 2004.

[46] Rehman I, Bonfield W. Characterization of hydroxyapatite and carbonated apatite by photo acoustic FTIR spectroscopy. Journal of materials science. 1997 Jan;8(1):1-4.

[47] http://www.nanotechnologyresearchfoundation.org/nanohistory.html

[48] Peter Hinterdorfer, Antoine Van Ojen Handbook of Single Molecule Biophysics

BIOGRAPHICAL INFORMATION

Tejaswi D. Kadapure was born in Maharashtra, India in January of 1989. She received her Bachelor of Engineering Degree in Biomedical Engineering from Watumull Institute of Technology, India in July 2010. To widen her horizons in the field of biomedical engineering research, she joined the Master of Science program in the Department of Bioengineering at the University of Texas Arlington in August 2010. The purpose of coming to America was served until she joined Dr. Nguyen's Nanomedicine and Tissue Engineering Lab, where she was exposed to a research environment she longed for. Under Dr. Nguyen's guidance, she was able to explore and conduct research on various drug delivery systems for the treatment of cancer, wound healing, and cardiovascular diseases. This experience in the field of research has created a different personality altogether for Tejaswi, who wishes to stay in the field of research throughout her career life.